Deformation of red blood cells using acoustic radiation forces

Puja Mishra, Martyn Hill, and Peter Glynne-Jones[a)]
Engineering Sciences, University of Southampton, Southampton SO17 1BJ, United Kingdom

(Received 7 April 2014; accepted 29 May 2014; published online 9 June 2014)

Acoustic radiation forces have been used to manipulate cells and bacteria in a number of recent microfluidic applications. The net force on a cell has been subject to careful investigation over a number of decades. We demonstrate that the radiation forces also act to deform cells. An ultrasonic standing wave field is created in a 0.1 mm glass capillary at a frequency of 7.9 MHz. Using osmotically swollen red-blood cells, we show observable deformations up to an aspect ratio of 1.35, comparable to deformations created by optical tweezing. In contrast to optical technologies, ultrasonic devices are potentially capable of deforming thousands of cells simultaneously. We create a finite element model that includes both the acoustic environment of the cell, and a model of the cell membrane subject to forces resulting from the non-linear aspects of the acoustic field. The model is found to give reasonable agreement with the experimental results, and shows that the deformation is the result of variation in an acoustic force that is directed outwards at all points on the cell membrane. We foresee applications in diagnostic devices, and in the possibility of mechanically stimulating cells to promote differentiation and physiological effects. © *2014 AIP Publishing LLC*. [http://dx.doi.org/10.1063/1.4882777]

I. INTRODUCTION

In recent years, mechanical stimulation[1,2] has been shown to be a key parameter in the differentiation of mesenchymal stem cells. This is especially relevant to regenerative medicine, and the growth of replacement tissue in bioreactors. In addition to influencing the differentiation of stem cells into different lineages, mechanical stimulation also has physiological effects such as accelerating ontogenesis.[3]

A number of strategies have been explored for applying mechanical stresses to cells including: using elastically deformable matrices, rotational moments applied through twisting magnetic beads, and compressing cells within a hydrogel matrix. However, these approaches are not ideal and frequently inhibit the free perfusion of media around a cell.

We present here an alternative based upon ultrasonic radiation forces—stresses that are applied directly to the cell membrane due to non-linear acoustic effects. The principle of acoustic deformation is demonstrated here on single cells that are acoustically levitated away from the device walls, however, it would also be possible to extend the concept to simultaneously act on millions of cells, and on cells cultured on surfaces. Red blood cells (RBCs) are used here as they are particularly compliant compared to other mamalian cells due to their spectrin cytoskeleton. By osmotically swelling the cells before the experiments, a spherical shape is created that makes small deformations easier to detect. In addition, osmotically swollen RBCs have been used by other investigators,[4,5] providing an important reference point for this study.

The mechanical stiffness of biological cells can also be used to distinguish cell types and for the identification of diseases.[6] For example, a malaria infected blood cell is known to be stiffer than a healthy normal blood cell.[7] Earlier studies have reported the deformation of RBCs

[a)]Author to whom correspondence should be addressed. Electronic mail: P.Glynne-Jones@soton.ac.uk

by applying a stretching force using optical tweezers,[4,5] where a pair of laser beams were used to trap a single RBC in suspension. An optical stress is exerted, causing an elongation of the cell body along the laser beam axis. However, optical tweezers are limited to manipulation of a small number of cells (ultrasonic manipulation can work with thousands of cells) and there is possibility of cell damage due to exposure to the high intensity optical field. Thus acoustic manipulation, which has been demonstrated to separate, filter, sort and mix biological cells,[8–11] has the potential to provide an alternative technique for cell deformation. In contrast to previous experimental studies, described below, acoustically deforming a cell using radiation forces is not straightforward because the cells have low acoustic contrast in their host medium and are small compared to the acoustic wavelength. To overcome these limitations, we describe here a system that uses a highly resonant cavity to achieve the required acoustic pressure amplitudes with little associated heating. There have been a number of studies investigating the effects of ultrasonic standing waves on cell viability and phenotype.[12] At low amplitudes, no significant effects are demonstrated during levitation.[13] At higher amplitudes effects can include cell death and sonoporation; however, our results indicate that even in cases where no adverse bio-effects are observed significant deforming forces can be generated.

In the past, a number of studies have been carried out to demonstrate deformation of small particles such as water droplets and bubbles using acoustic radiation force. In particular, experimental and theoretical investigations were focused on understanding the phenomena and mechanisms of droplet deformation and breakup. Experimental studies have reported that the equilibrium shape of the particle can be significantly deformed from their initial spherical shape.[14,15] Marston presented a theoretical approach to calculate the shape of a droplet, deformed by a standing wave field in one dimension:[16] the scattered wave and resulting radiation stresses on the interface were calculated for small deformations from a spherical shape. Jackson *et al.*[17] extended Marston's theory to a three-dimensional sound field, included gravity acting on the droplet as a factor affecting deformation, and wrote final expressions that were valid for particles of any size, though still only valid for small deformations.

The acoustic scattering by a non-spherical object was first included by Tian *et al.* to determine the static deformation of an acoustically levitated drop in air.[18] Approximations limited this approach to deformed aspect ratios of less than two.[19] A number of experimental studies also supported the analytical approach, for example, Trinh and Hsu[15] quantified the deformations of droplets of a range of liquids. Anilkumar *et al.*[20] studied droplet deformation until breakup in order to determine the threshold of drop integration.

Numerical studies have also investigated particle deformation. Lee *et al.* developed a numerical method to study the drop instability and static deformation in a disk model.[21] Shi and Apfel[22] reported another numerical method to study the static shape deformation of a liquid drop in a gaseous environment. The method calculated the exterior sound field by solving the line integral form of wave equation which estimated the stress profile along the drop meridian accurately. The numerical results compared well with the experimental results by Tian *et al.*[18] and analytical results for small deformation range.[16] However, study was restricted to the condition when the inside liquid has high acoustic impedance compared to the outside and therefore, is not suitable for biological cases where the particle and medium have similar acoustic properties.

To support our experimental results, we model cell deformation using an efficient finite element method[23] that is valid for a cell of any size relative to the acoustic wavelength. An iterative, moving mesh method is used that makes the results valid for large deformations.

II. MATERIALS AND METHODS

A. Design and characterisation of acoustic device

Our acoustic device for producing cell deformation is based around a square glass microcapillary with internal dimensions 100 μm $\times$ 100 μm, and wall thickness 50 μm (VitroCom #8510, Mountain Lakes, NJ) as shown in Figure 1. The capillary forms a resonant cavity in which an ultrasonic standing wave is formed. The resulting resonance (as discussed below)

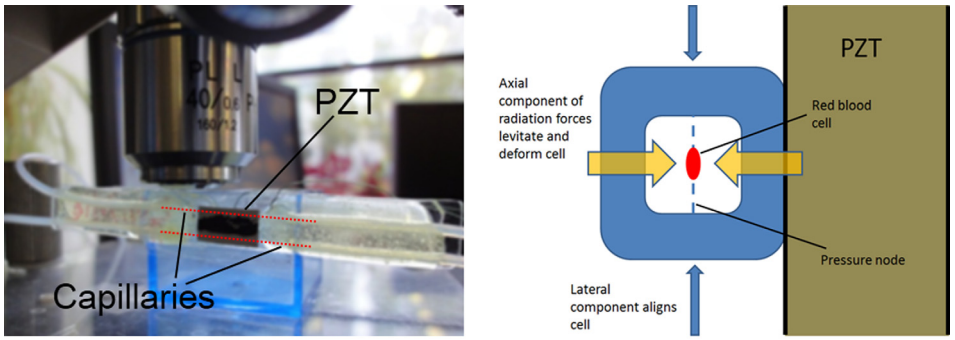

FIG. 1. (a) Experimental device under the microscope. This device has two parallel capillaries (only one used at a time), which are too small to be seen, but indicated by the red-dashed lines. The black marks are ink to reduce reflections that interfere with the imaging. (b) Schematic diagram of the device showing a cell being levitated and deformed by the axial acoustic radiation forces (see Figure 2 for a more detailed indication of the acoustic field). The cavity has a width and height comparable to a half wavelength at the operation frequency. Differences between the acoustic radiation pressure on the inner and outer surfaces of the cell membrane cause deformation. Smaller lateral gradients in the velocity field align the cell in the centre of the channel.

both manipulates cells to the centre of the capillary (permitting easier visualisation and repeatable experimental results) and also creates the deforming force that is the subject of this paper. The ultrasound is excited by a 1 mm thick plate of PZT (PZ27, Ferroperm, Kvistgaard, Denmark) of dimensions 15 mm × 8 mm glued to the capillary using epoxy (Epotek 301) applied in a thin layer using an absorbent pad, and cured in an oven at 120 °C for 1 h. Two such capillaries were glued parallel to the long sides of the PZT, about 1 mm from each edge (this creates 2 resonant chambers, only one is characterized and used in the following). The glue layer was measured as being ∼10 μm thick. For ease of handling, the assembly was mounted using adhesive tape to a glass microscope slide, with glass spacers under the PZT to ensure the acoustic resonance is not disrupted. PTFE tubing (ID 0.3 mm) was pushed ∼1 cm over each end of the capillary and sealed with epoxy to enable samples to be introduced. It was found that small variations in pressure and tube position induced unwanted flow in the chamber (experiments are carried out at zero flow rate). To prevent this, the tubes from each capillary were led to two reservoirs (5 ml glass bottles) whose fluid levels could be adjusted until no flow was found across the device. Blood (see below) was introduced into one of the reservoirs, and caused to flow through the device by pressurizing the air above the fluid using a 3 ml syringe filled with air connected to the lid of the reservoir by a luer connector glued into the lid.

A 2D acoustic model of the acoustic resonance in the capillary, shown in Figure 2, was produced in COMSOL, modelling the fluid cavity excited by a normal acceleration of the

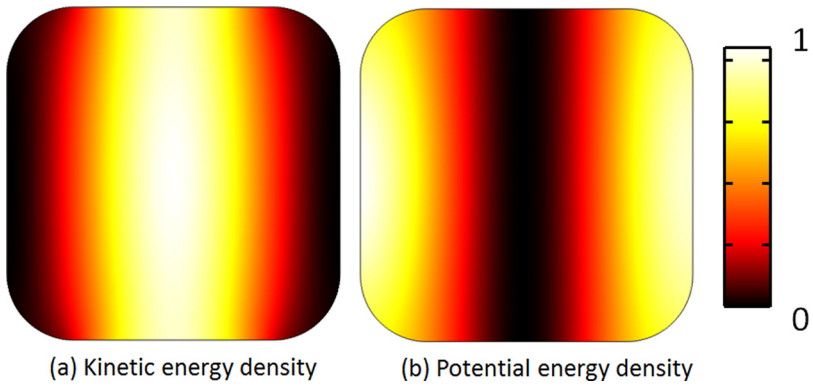

FIG. 2. The modelled acoustic mode in the capillary at a model resonance of 7.6 MHz. Cells experience gradient forces both towards the kinetic energy maximum, and potential energy minimum, forming a 2D trap that holds the cell in the centre of the capillary. Arbitrary units.

right-hand wall (properties as listed in Table I). We acknowledge that other acoustic modes can be produced in the capillary with different boundary conditions; however, this mode matches well the experimentally observed radiation forces in our system inferred from observing blood-cell movements, with cells experiencing forces both horizontally and vertically towards the centre line of the capillary resulting from gradients in the potential and kinetic acoustic energy densities respectively. More detailed description of the modelling method, and discussion of how the gradients in average acoustic energy densities give rise to this effect can be found in our previous work.[24] It is the small gradient in the kinetic energy density along the pressure nodal line that creates the vertical (lateral) components of the force that holds the cell in the centre of the channel. In practice, the 3D nature of the real device and complex geometrical structure produces some regions that behave as predicted in this model and others that do not, presumably due to 3D resonances and flexural motion of the capillary walls.

Experimentally, the resonant frequency was established by exploring the frequencies in the vicinity of the resonance predicted using the 2D numerical model. 10 μm fluorescent polystyrene beads (Polysciences #18140-2) were introduced and observed as a range of frequencies are applied to the device (because there is a relatively small level of electromechanical coupling between the PZT and cavity resonance the resonances cannot be found by inspecting the electrical impedance spectrum). The PZT was driven by an RF-amplifier (ENI 240L) driven by a sine-wave from a signal generator (TTi TG1304). At 7.900 MHz, a strong half-wave resonance is found such that particles are both levitated and focussed laterally into a single line down the centre of the capillary.

Optical phase contrast microscopy was used to view the deformation of blood cells using a phase contrast objective (40× magnification, numerical aperture 0.6). The device was mounted with the PZT plate off the optical axis, so that blood cells could be observed through the side of the capillary, which provides a profile view of the deformation. A view normal to the transducer (which would also prevent transmitted illumination) would only show a change in apparent size of the red blood cell as it is deformed. This would be difficult to distinguish from changes in apparent cell size caused by the changes in the position of the cell relative to the focal plane of the objective. The phase contrast between the blood cell and host fluid solution creates a dark ring around the boundary of each cell, allowing easier measurement of its deformation. However, the illumination path is partially obstructed by the transducer, reducing the clarity of the resulting image.

Measuring the acoustic pressure amplitude within the resonant cavity is difficult due to the confined space. The acoustic pressure amplitude inside the capillary for a given drive voltage was found by balancing the weight of a 10 μm fluorescent polystyrene bead against the acoustic radiation force in the manner described by Spengler *et al.*[25] Acoustic pressure was found to be related to drive voltage applied to the PZT by a factor of 26 kPa/Vpp ± 20%. The low accuracy of this measurement is caused by the difficulty of ascertaining when the two forces are precisely balanced, and uncertainty in the material properties of the polystyrene beads.

B. Preparation of blood cells

Fresh rat blood was obtained as a waste product from other experiments. Blood was removed by cardiac puncture from rats immediately following cervical dislocation. The blood was mixed with Lithium Heparin at 20 IU/ml. Experiments were carried out within 48 h of blood collection. The blood was centrifuged at 2000 rpm for 5 min, and the plasma and buffy

TABLE I. Parameters used in the modelling.

Cell radius	3.1 μm (Ref. 5)	Frequency	7.9 MHz
Cell density	1139 kg m^{-3} (Ref. 28)	Speed of sound in cell	1680 ms^{-1} (Ref. 29)
Medium density	1000 kg m^{-3}	Speed of sound in medium	1480 ms^{-1}
Cell membrane Young's modulus, E	629 Pa (Ref. 5)	Cell membrane Poisson's ratio	0.499 (Ref. 5)

coat removed by Pasteur pipette. 50 μl of the centrifuged blood was mixed with 5 ml of a hypotonic solution of 50% PBS buffer (Sigma Aldrich #P4417) with 50% de-ionized water and placed in the acoustic device's reservoir. The resulting osmotic uptake of water by the cells changes their morphology from the familiar bi-concave disc to a spherical shape.[5] All results in this paper are presented for this hypotonic medium, with a calculated osmolality of 148 mOsm and haematocrit of 0.5%. Experiments were conducted at room temperature (around 20 °C).

C. Measurement of cell deformation and image processing

In order to extract, cell shape images were processed in MATLAB using an algorithm similar to that presented by Guck.[5] For each cell, the algorithm first used a polar-to-rectangular projection about the image centre (i.e., the image is "unwrapped") to map the cell boundary to a line crossing the image. Next, the boundary was designated as the point of minimum intensity (the centre of the black ring created by the phase-contrast). The boundary was smoothed by taking a spatial Discrete Fourier Transform (DFT) and discarding all but the eight lowest frequency components before recombining them with an inverse FFT. The smoothed data was then mapped back to its polar form. Finally, the resulting data were fitted to an ellipse using a least squares method. The length of semi-major and semi-minor axis of the fitted ellipse represent the diameters of the deformed cell, and the aspect ratio is calculated as the ratio between them, with an aspect ratio greater than one representing a cell that has been compressed along the same axis as the one seen in Figure 1.

III. THEORY AND NUMERICAL MODELLING

Numerical modelling is used here to demonstrate that the observed deformations are in accord with those that would be created by the theory of acoustic radiation force, and to explore the physical mechanism and typical force distributions on the membrane.

A. Acoustic radiation stresses

Throughout an acoustic field, a non-zero time-averaged stress is created by non-linear terms in the Navier-Stokes equations. This stress is discontinuous across the boundary of a cell and its effect can be approximated in the non-viscous regime as a stress difference.[16,26]

$$\Delta\Pi = \Pi_i - \Pi_o, \tag{1}$$

where Π_i and Π_o are the stresses resulting from the acoustic radiation stresses on the inside and outside of the membrane, respectively, given to second order as[27]

$$\Pi_{jk} = -\langle P - P_0\rangle\delta_{jk} - \rho_0\langle v_j v_k\rangle, \tag{2}$$

where δ_{jk} is the Kronecker delta, $<\ldots>$ represents the time average, and the time average excess pressure is given by

$$\langle P - P_0\rangle = \frac{1}{2\rho c^2}\langle p^2\rangle - \frac{\rho}{2}\langle v^2\rangle, \tag{3}$$

where p and v are the first order acoustic pressure and velocity. Thus in the inviscid approximation, it is possible to express the second order radiation stresses in terms of the first order acoustic field variables, leading to a simplified computational method.

B. Numerical implementation

Finite element models were implemented in 3D in COMSOL multi-physics (version 4.3), a commercial multi-physics finite element method package. The advantage of Eqs. (1)–(3) above is that in the non-viscous approximation the acoustic radiation stress is a function of the first

order acoustic fields. This means that it is possible to decouple the problem into a sequence of steps rather than solving the whole system of equations simultaneously. The deformed shape is found iteratively by successively repeating three steps until equilibrium is reached:

(1) A linear acoustic model predicts the pressure and velocity distributions on the inner and outer surfaces of the red blood cell. In this step, both the inside of the cell and the surrounding fluid are modelled by acoustic regions, using the properties given in Table I. A non-slip condition is imposed at the boundary. Only a small region in the vicinity of the cell is modelled, with a radiation boundary condition around the model boundary used to both create the acoustic field and absorb incident radiation. We have previously described this arrangement in more detail,[23] and shown it to produce accuracies of better than 1%. The osmotically swollen red blood cell is modelled as initially having a spherical shape.
(2) The acoustic radiation stresses resulting from the first order acoustic field found in step 1 are calculated using Eq. (1). The COMSOL operators *up()* and *down()* are required to extract the acoustic field components on either side of the boundary. These stresses are applied to our mechanical model of the red-blood cell (see below) to predict its deformation.
(3) An arbitrary Lagrangian-Eulerian (ALE) moving mesh (COMOSL's built-in implementation) tracks the induced movement of the blood cell membrane and creates a deformed geometry that is used as an input step for the next iteration, thus allowing for non-linear deformations.

Although this sequence could be used to predict the dynamic behaviour of the blood cell's deformation, we did not attempt this at this stage, as it would require the inclusion of the fluid motion in and around the blood cell with correspondingly extended computation times, and more difficulty in achieving numerically stable results. The mechanical model of the blood cell comprised a thin shell structure. This formulation allows for both membrane stresses, and bending stresses, however, the material properties (listed in Table I) mean that membrane stresses dominate the behaviour. Since in the mechanical model used in step 2, we did not model the fluid inside the cell, we included an artificial volume dependent pressure on the membrane, added to the acoustic stress, in order to constrain the volume of the cell to be constant. This took the form,

$$p_{vol} = K\frac{(V_{cell} - V_0)}{V_0}, \tag{4}$$

where V_0 and V_{cell} are the original and deformed volume, respectively, and K an arbitrary constant, set to 1 kPa. With this constraint the cell volume was found to vary by no more than 0.5% from its initial value in the models presented here. Mechanical damping in the shell did not affect the ultimate deformed shape—higher damping merely increased the number of modelling steps required to reach equilibrium, thus we were able to choose a value that gave reasonable numerical stability. At higher amplitudes, stability remains challenging, limiting our ability to model the full range of experimental conditions.

In order to verify our mechanical model of the cell membrane, we compared it to the analytic model described by Guck.[5] We applied a radially directed stress distribution (as calculated by Guck) of

$$\sigma_r(\theta) = \sigma_0 \cos^2(\theta), \tag{5}$$

where θ is the surface elevation in polar coordinates, and found good agreement with his modelled shape deformations for σ_0 in the range 0.5 to 2.5 Pa. In this case, we did not constrain the cell volume to be constant as Guck's model did not do this. Applying this constraint resulted in deformations that were approximately 50% smaller.

IV. RESULTS AND DISCUSSION

Blood cells were trapped one at a time in the active region of the capillary, and subjected to a range of pressure amplitudes. Figure 3 shows an image of a typical deformed cell within

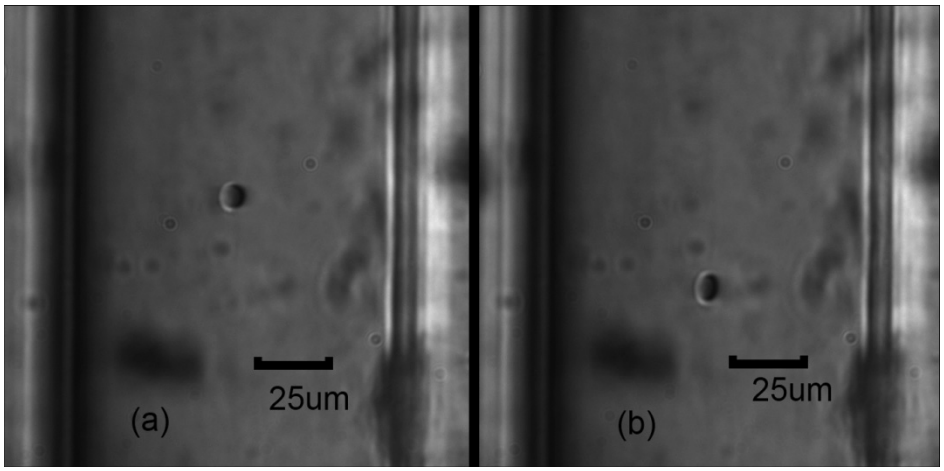

FIG. 3. Deformation induced by acoustic radiation forces for an osmotically swollen red blood cell. The walls of the capillary can be seen on either side of each image. (a) Low acoustic pressure amplitude levitates cell. (b) Deformed cell at a pressure amplitude of 978 kPa.

the capillary. Some translational movement is also seen due to both residual fluid movement (even small pressure fluctuations in the reservoirs induces flow), and lateral acoustic radiation forces. Figure 4 shows a sequence of a deformed blood cell images for a range of acoustic pressure amplitude from 12.9 kPa to 978 kPa, with fitted ellipses. It can be clearly observed that increasing pressure amplitude results in increasing amounts of cell deformation towards an ellipsoid. For each of $n = 8$ blood cells, a sequence of acoustic pressures was applied by varying the drive voltage. Cells were given 10 s at each pressure amplitude to come to equilibrium before the corresponding image was captured for processing. The results were obtained by stepping each cell through a sequence of amplitudes beginning with the lowest. It was found that the deformation of each cell was reversible—stepping back through the amplitudes resulted in deformations indistinguishable from those measured on the way up (to within the measurement errors of our system, found to be around ± 0.1 for the aspect ratio). The deformation occurred more quickly than could be seen by the eye. We did not investigate this dynamic behaviour, but Baskurt and Meiselman[30] measured the relaxation time of shape deformations to be of order 100 ms. The temperature of the transducer was measured—at the highest pressure amplitude a temperature rise of around 1 °C was measured on the capillary surface above the transducer. If this technique were to be incorporated into a system which required maintenance of physiological temperatures, this modest rise could be counteracted by reducing the ambient temperature of the system.

Figure 5 shows the average change in aspect ratio vs acoustic pressure amplitude. It can be seen that the deformations are comparable to those found under the action of optical forces; Guck reports optical deformations of osmotically swollen RBCs up to aspect ratios of around 1.5.[5]

It would be possible to question whether the observed changes in aspect ratio were instead due to the rotation of a blood cell of fixed bi-concave shape. However, there are two reasons to discount this possibility:

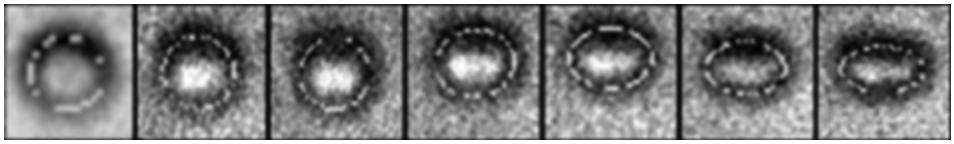

FIG. 4. Images showing a single osmotically swollen red blood cell under the influence of a range of acoustic pressure amplitudes from 0–978 kPa (going left to right). White line shows fitted ellipse.

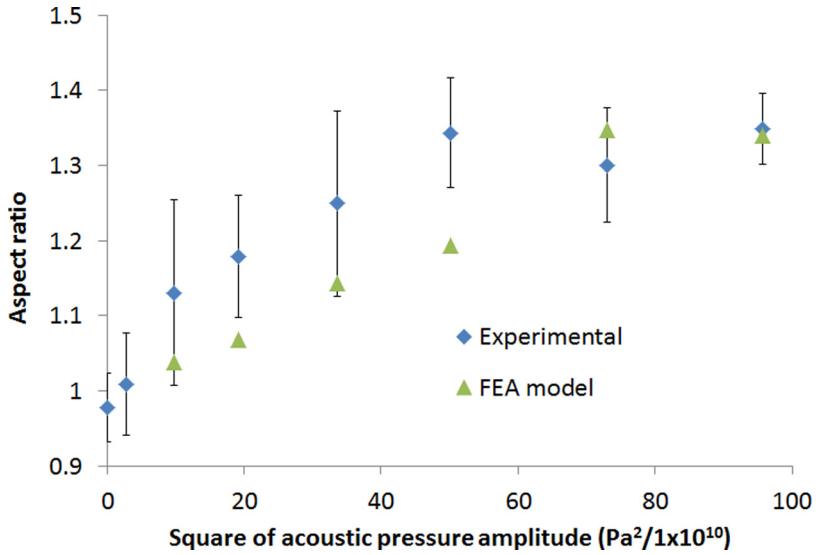

FIG. 5. Aspect ratio of the deformed blood cell shape with varying acoustic pressure amplitude. Error bars shows range of measurements over a sample of n = 8 cells. Note that the measured pressure amplitude is subject to a systemic error of ±20%.

(a) All observed cells were found to cycle in shape with pressure. At zero pressure amplitude no cells (out of hundreds observed), appeared deformed (indicating successful osmotic swelling).
(b) It has been observed[31] that RBCs of a bi-concave shape naturally align themselves (even at low acoustic amplitudes) such that the plane of the disc is in the pressure nodal plane of the standing wave field. We confirm this finding, and note that this would cause (non-spherical) cells to appear with high aspect ratio at low pressure amplitudes, which is not observed.

It is difficult to attain close correspondence between the measured and modelled cell deformation due to uncertainty in the measurement of the experimental acoustic pressure amplitude (±20%) inside the capillary. However, allowing for this uncertainty the modelled results, shown in Figure 5 are in accord with the measured deformations. The modelled result is consistently at the lower end of the measured range, and we speculate that there may be some systematic errors causing this difference. Possibilities include: (a) errors in the optical measurement of shape, since the cell boundary does not correspond exactly with the minimum in the phase-contrast image; and (b) it has been found that acoustic streaming patterns can influence cell shape.[32] Streaming was observed to be occurring in the capillary (occasional pieces of cell debris were seen to rotate whilst trapped), however, we were unable to quantify it as our 0.5 μm diameter tracer beads were concentrated by the radiation forces due to the relatively high excitation frequency. An additional source of the variation that is observed experimentally will come from the variability of the mechanical properties of the RBCs themselves (for example Chabanel *et al.*[33] show standard deviations of around 10% in the elastic moduli of membranes).

It is instructive to examine the force distribution around the cell surface as predicted by the model. In the following discussion we define the cell equator as the region whose normals point perpendicular to the axis of acoustic propagation (the "axial" direction), and thus lies in the acoustic pressure nodal plane. Figure 6(a) shows the distribution of forces on both an undeformed cell, and the same cell at equilibrium at an acoustic pressure amplitude of 650 kPa. It can be seen that the acoustic radiation forces exert a net *outward* stress at all points over the surface of the cell. However, the outward stress is larger at the equator of the cell, resulting in a net stretching along the acoustic pressure nodal plane. The internal forces produced by the requirement that cell volume is preserved are thus important in causing the polar regions to be deformed inwards. Interestingly, the radiation force induced on the membrane is not strongly affected by the deformation seen here.

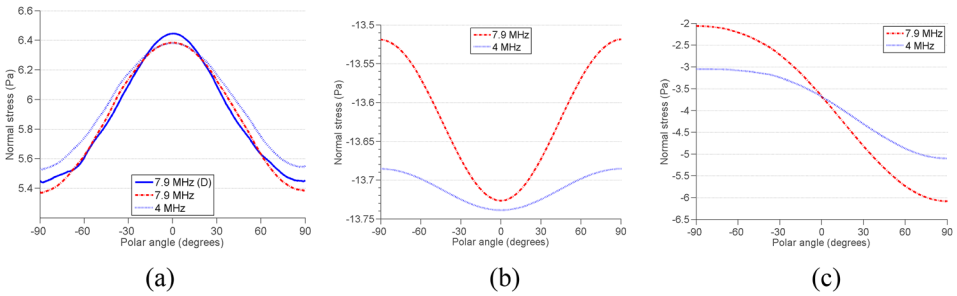

FIG. 6. The normal component of acoustic radiation pressure on the surface of a red blood cell (the polar angle is zero at the equator) for an acoustic pressure amplitude of 650 kPa. In each plot values for both the experimental frequency of 7.9 MHz and 4 MHz are shown. Radiation pressures are shown on undeformed cells, except for the trace "7.9 MHz (D)", which is for the cell in its deformed state. (a) For a cell positioned at the pressure node as seen in our experiments; (b) for a cell at the pressure anti-node; (c) for a cell halfway between these locations. In each case, results for two frequencies are presented: 4 MHz and 7.9 MHz. A positive value denotes an outwardly directed force.

At the polar regions, all velocities are directed normal to the cell surface, so it is possible to combine the terms in Eq. (1) and express the resulting normal stress as a pressure difference,

$$\triangle P = \frac{1}{2}(\rho_o - \rho_i)\langle v^2\rangle + \frac{1}{2}(\beta_o - \beta_i)\langle p^2\rangle, \tag{6}$$

where we have also taken advantage of the acoustic pressure and velocities being continuous across the boundary.

Similarly at the equator where the normal acoustic velocity components and pressure are both zero,

$$\triangle P = -\frac{1}{2}\rho_o\langle {v_o}^2\rangle + \frac{1}{2}\rho_i\langle {v_i}^2\rangle. \tag{7}$$

Note the change of sign in the velocity contributions between these two equations. The terms relate to the differences in the kinetic and potential energy densities of the acoustic field either side of the cell membrane.[24] In the current device, the cell is levitated at a pressure node so the pressure dependent terms are dominated by the much larger velocity (kinetic energy) terms. Thus, the velocity terms whose net effect depends on both the difference in density and the difference in velocity on either side of the membrane are seen to be the important parameters. Figure 7 shows a typical velocity distribution around a deformed cell. It can be seen that the magnitude of the fluid velocity is greater around the equator, which can be thought of in terms of the nearly incompressible medium flowing around the cell. Examining the contributions made by the various terms in Eqs. (1)–(3), it is found that at the equator this increased velocity is more significant than the contribution resulting from the differing densities between the cell and the medium.

In acoustic particle manipulation where it is the net force on the particle that is of interest, forces are proportional to the gradients in acoustic energy densities.[34] In derivations of these net forces, the "deforming" forces calculated here, which have zero resultant force on the cell as a whole can be neglected.[35] The net forces scale linearly with frequency for a given pressure amplitude, as the energy gradients increase. In contrast, the deforming forces do not depend on the gradients of the field quantities, and while there is a complex interplay of parameters as the frequency changes, there is not a clear trend of force variation with frequency. For example, Figure 6 illustrates the force distributions at two excitation frequencies for cells in three positions: (a) at the pressure node, as found in our experiments; (b) at the pressure anti-node; (c) half-way between these positions (a cell at this location experiences the maximum manipulation force). It can be seen that for a levitated cell in position (a), the excitation frequency has only a small effect, compared to the other cases. It is interesting to note that a cell on a rigid surface

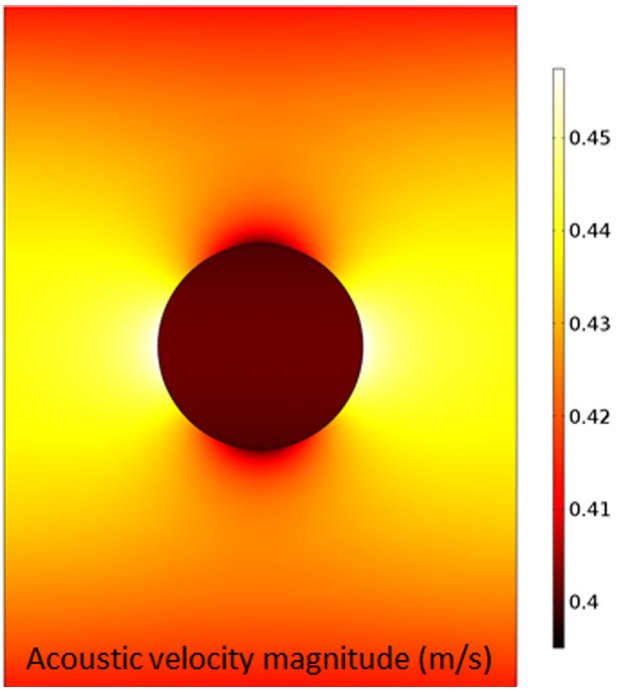

FIG. 7. The distribution of the magnitude of the acoustic velocity around a levitated cell (undeformed) at incident pressure amplitude 650 kPa.

would typically experience acoustic conditions similar to that in case (b), which result in much smaller deforming forces. In case (c), the pressure distribution is not symmetrical about the cell equator since there is a net-force on the cell (integrating this pressure over the whole surface has been verified to yield the net force predicted by Gor'kov's formula[34]).

V. CONCLUSIONS

Ultrasonic standing wave fields have been shown to be capable of inducing deformations in red blood cells that are comparable to those demonstrated by optical methods, with little measured heating. This has promising applications in both diagnostic and tissue engineering systems. Modelling has shown that acoustic radiation forces can be considered the primary mechanism for cell deformation, and that the resulting force distribution is comparable to an outwardly directed pressure that is greater on the portion of the cell in the acoustic nodal plane. It has also predicted that the forces experienced by cells on surfaces will be of a lower magnitude. By changing the device configuration to a planar arrangement, there is the possibility of applying mechanical stimulation to millions of cells simultaneously; in this case, the planar arrangement would give rise to a more uniform field than that found in the capillary, further strengthened by the propensity of cells to agglomerate at regions of maximum kinetic energy density. Further work will seek to explore these configurations, and demonstrate enhanced outcomes in tissue engineering applications.

ACKNOWLEDGMENTS

The authors gratefully acknowledge the financial support for this work received from the EPSRC under the Sonotweezers project (EP/G012075/1).

[1]A. J. Engler, S. Sen, H. Lee Sweeney, and D. E. Discher, Cell **126**(4), 677 (2006).
[2]N. D. Evans, C. Minelli, E. Gentleman, V. LaPointe, S. N. Patankar, M. Kallivretaki, X. Y. Chen, C. J. Roberts, and M. M. Stevens, Eur. Cells Mater. **18**, 1 (2009).
[3]P. Leucht, J.-B. Kim, R. Wazen, J. A. Currey, A. Nanci, J. B. Brunski, and J. A. Helms, Bone **40**(4), 919 (2007).

[4]A. Korobtsov, S. Kotova, N. Losevsky, A. Mayorova, V. Patlan, E. Timchenko, N. Lysov, and E. Zarubina, Laser Phys. **22**(7), 1265 (2012).
[5]J. Guck, R. Ananthakrishnan, H. Mahmood, T. J. Moon, C. C. Cunningham, R. Hallworth, and J. Kas, Biophys. J. **80**(1), 277A (2001).
[6]S. Suresh, Acta Mater. **55**(12), 3989 (2007).
[7]C. Li and K. K. Liu, J. Mater. Sci.-Mater. Med. **19**(4), 1529 (2008).
[8]A. Lenshof, C. Magnusson, and T. Laurell, Lab Chip **12**(7), 1210 (2012).
[9]P. Glynne-Jones, R. J. Boltryk, and M. Hill, Lab Chip **12**, 1417 (2012).
[10]T. Franke, S. Braunmuller, L. Schmid, A. Wixforth, and D. A. Weitz, Lab Chip **10**(6), 789 (2010).
[11]J. Nam, H. Lim, D. Kim, and S. Shin, Lab Chip **11**(19), 3361 (2011).
[12]M. Wiklund, Lab Chip **12**(11), 2018 (2012).
[13]D. Bazou, R. Kearney, F. Mansergh, C. Bourdon, J. Farrar, and M. Wride, Ultrasound Med. Biol. **37**(2), 321 (2011).
[14]R. G. Holt and L. A. Crum, "Acoustically forced oscillations of air bubbles in water: Experimental results," J. Acoust. Soc. Am. **91**, 1924 (1992).
[15]E. H. Trinh and C. J. Hsu, J. Acoust. Soc. Am. **79**(5), 1335 (1986).
[16]P. L. Marston, J. Acoust. Soc. Am. **67**(1), 15 (1980).
[17]H. W. Jackson, M. Barmatz, and C. Shipley, J. Acoust. Soc. Am. **84**(5), 1845 (1988).
[18]Y. R. Tian, R. G. Holt, and R. E. Apfel, J. Acoust. Soc. Am. **93**(6), 3096 (1993).
[19]T. Hasegawa and K. Yosioka, J. Acoust. Soc. Am. **46**, 1139 (1969).
[20]A. V. Anilkumar, C. P. Lee, and T. G. Wang, Phys. Fluids A-Fluid Dyn. **5**(11), 2763 (1993).
[21]C. P. Lee, A. V. Anilkumar, and T. G. Wang, Phys. Fluids **8**(10), 2580 (1996).
[22]W. T. Shi and R. E. Apfel, J. Acoust. Soc. Am. **99**, 1977 (1996).
[23]P. Glynne-Jones, P. P. Mishra, R. J. Boltryk, and M. Hill, J. Acoust. Soc. Am. **133**(4), 1885 (2013).
[24]P. Glynne-Jones, C. Démoré, C. Ye, Y. Qiu, S. Cochran, and M. Hill, IEEE Trans. Ultrason. Ferroelectr. Freq. Control **59**(6), 1258 (2012).
[25]J. F. Spengler, M. Jekel, K. T. Christensen, R. J. Adrian, J. J. Hawkes, and W. T. Coakley, Bioseparation **9**(6), 329 (2001).
[26]P. V. Zinin and J. S. Allen, "Deformation of biological cells in the acoustic field of an oscillating bubble," Phys. Rev. E **79**, 021910 (2009).
[27]C. P. Lee and T. G. Wang, J. Acoust. Soc. Am. **94**(2), 1099 (1993).
[28]M. Godin, A. K. Bryan, T. P. Burg, K. Babcock, and S. R. Manalis, Appl. Phys. Lett. **91**(12), 123121 (2007).
[29]L. Gherardini, C. M. Cousins, J. J. Hawkes, J. Spengler, S. Radel, H. Lawler, B. Devcic-Kuhar, and M. Groschl, Ultrasound Med. Biol. **31**(2), 261 (2005).
[30]O. K. Baskurt and H. J. Meiselman, Biorheology **33**(6), 489 (1996).
[31]W. T. Coakley, D. Bazou, J. Morgan, G. A. Foster, C. W. Archer, K. Powell, K. A. J. Borthwick, C. Twomey, and J. Bishop, Colloid Surf. B-Biointerfaces **34**(4), 221 (2004).
[32]M. Lokhandwalla and B. Sturtevant, Phys. Med. Biol. **46**(2), 413 (2001).
[33]A. Chabanel, D. Schachter, and S. Chien, Hypertension **10**(6), 603 (1987).
[34]L. P. Gor'kov, Sov. Phys. Dokl. **6**(9), 773 (1962).
[35]K. Yosioka and Y. Kawasima, Acoustica **5**, 167 (1955).